IEEJ Journal of Industry Applications
Vol.7 No.5 pp.410–415 DOI: 10.1541/ieejjia.7.410

Paper

Implementation of Decoupling Power Flow Control System in Triple Active Bridge Converter Rated at 400 V, 10 kW, and 20 kHz

Koya Nishimoto* Non-member, Yuichi Kado*a) Non-member
Keiji Wada* Senior Member

(Manuscript received July 31, 2017, revised Jan. 23, 2018)

An autonomous DC microgrid system that uses a triple active bridge (TAB) converter as a power routing unit is proposed. A control system that can independently manage the current and voltage of each port is needed to construct the microgrid. This paper describes how the decoupling power flow control system is implemented in the prototype TAB converter rated at 400 V, 10 kW, and 20 kHz. The validity of the system was demonstrated by measuring the step response of the TAB converter. The experimental results showed that the system provided the designed dynamic characteristics from the viewpoints of output current control and constant voltage control. Decoupling power flow control between each port was also achieved.

Keywords: three-way power router, triple active bridge converter, phase shift modulation, decoupling control, power flow control, autonomous microgrid system

1. Introduction

To ensure the security of self-sufficient energy supplies and to prevent climate change, we need to achieve an autonomous DC microgrid system that can promote local power generation for local power consumption [1]–[11]. To construct a DC microgrid with a large number of renewable energy sources, the demand and supply balance of the power in the microgrid must be adjusted by utilizing energy storage. Furthermore, this microgrid system will need to be easy to construct, extend, and maintain at low cost.

In response to these requirements, we propose a three-way power router that can be used as a unit cell of a microgrid composed of a triple active bridge (TAB) converter and AC/DC converters that can be connected to each I/O port of the TAB converter. Hence, the power router can manage both AC and DC power [11].

When the microgrid is constructed with a three-way power router, the control objective of each port should change depending on the situation, as shown in Fig. 2. All ports' voltages have to be kept constant to drive the TAB converter. Therefore, when the two TAB converters are connected through the DC bus, one has to control the DC voltage at least, as shown in Fig. 2. By having one control the voltage, the other one can control the current through the DC bus, that is, the transmission power in a microgrid becomes controllable. When the load is connected to one port of the TAB converter, the output voltage of that port has to be constant to supply energy stably. Besides, when the global grid is connected through the AC/DC converter, the TAB converter can control the output current because the voltage of the port is controlled by the AC/DC converter. The batteries are important components in the microgrid. They work as an energy buffer in the grid because they can absorb and supply the energy. Voltage control and current control are necessary functions to construct the microgrid with TAB converters.

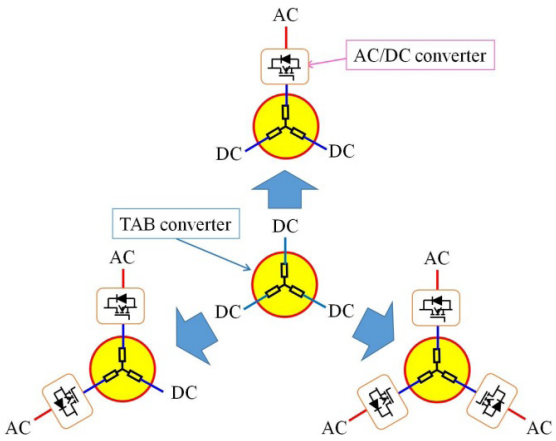

Fig. 1. Three way power router

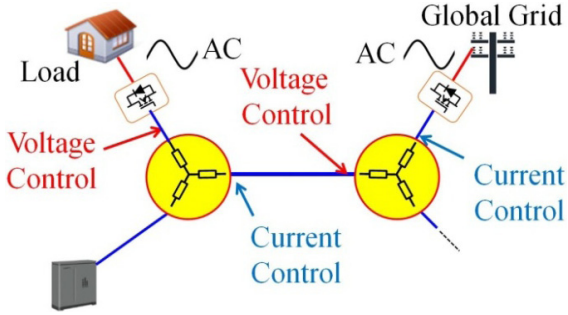

Fig. 2. Variety of controls

a) Correspondence to: Yuichi Kado. E-mail: kado@kit.ac.jp
* Kyoto Institute of Technology
Matsugasaki, Sakyo-ku, Kyoto 606-8585, Japan

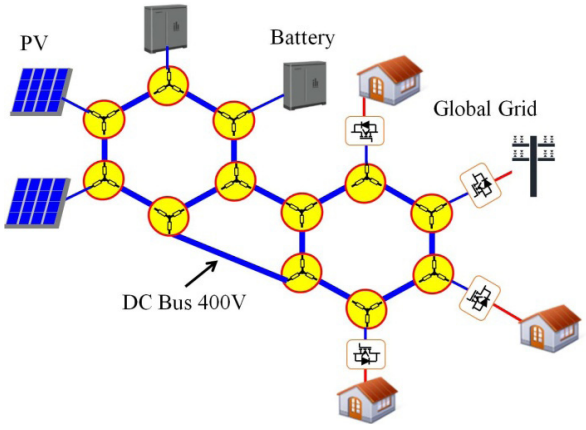

Fig. 3. An autonomous DC microgrid system

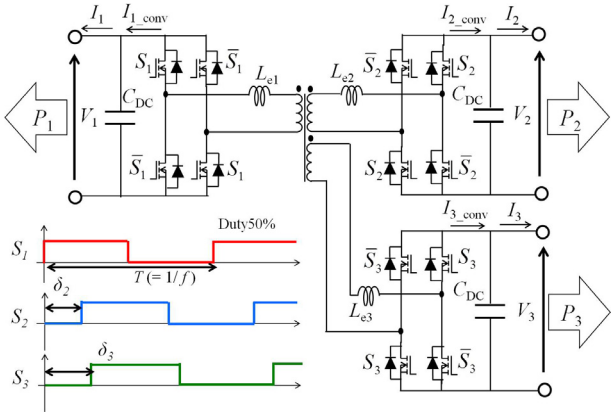

Fig. 4. Circuit configuration of TAB converter

Figure 3 shows an autonomous DC microgrid system consisting of TAB converters. In a grid system, power flow is controlled by TAB converters, and demand and supply balance can be adjusted by controlling the transmission power of TAB converters between three ports. The DC microgrid we proposed has a larger amount of loss than the typical DC microgrid with DAB converter. However, the ease of expansion and the reliability of the power supply are advantages.

First, the power supply system needs to have very high reliability during disasters. The microgrid we proposed can have several transmission lines for power supply. In addition, each DC bus in Fig. 3 is isolated with a three-winding transformer in a TAB converter. If a short-circuit fault occurs in a DC bus, only the fault bus is affected owing to the isolation. Namely, the microgrid can keep operating even if the some buses have a short circuit fault.

Second, the microgrid should be extended easily. Furthermore, power supply to the consumer must not be stopped during the construction. As shown in Fig. 2, the transmission power through each bus can be controlled actively by TAB converters. That is, the transmission power through the bus at the construction point can be regulated at zero current, and it can be disconnected safely. In addition, because the microgrid has several transmission lines, power can be continually supplied. Namely, the construction can be carried out safely, and the power supply does not need to be stopped.

The voltage drop problem in the DC bus is also a critical issue for the DC microgrid with DAB converters and the common DC bus. DC voltage regulators such as batteries and fuel cells have to be installed in the appropriate point to regulate the voltage in the DC bus [12]. Therefore, the place and number of voltage regulators must be considered again when the structure of the microgrid is changed to respond to the variation in demand. In contrast, for the microgrid with the TAB converter shown in Fig. 3, voltage regulators for each DC bus are not necessary because one of the TAB converters at both ends of a DC bus controls the voltage. Therefore, the microgrid can be expanded and contracted flexibly.

Difficulty occurs in matching the transmission power with the command value in a microgrid with a large number of converters due to some disturbances such as dependency of overall loss in the converter [13] and parameter dispersion of passive elements. Moreover, the transmission power of one port in the converter interferes with other ports.

Therefore, this paper presents a decoupling power flow control system including current control and voltage control. Then, it describes the system implementation in the prototype TAB converter and shows a demonstration of the system's validity in a measurement of the step response. The rest of this paper is organized as follows. Section 2 explains the circuit configuration of the TAB converter, which is a basic component of the three-way power router, and basic equations for power flow control. Section 3 explains the decoupling power control system of the TAB converter and details how the closed-loop transfer function of the system is derived from basic equations. The implementation method of the system in the prototype TAB converter is described in Section 4. The experimental results for the prototype with the system, rated at 400 V and 10 kW, are presented in Section 5. We conclude with a brief summary in Section 6.

2. Basic Equations

The circuit configuration of the TAB converter [14][15] is shown in Fig. 4. The TAB converter consists of full bridge inverters, external inductors, and a three-way transformer. Here, f_{sw} is the switching frequency of gate control signals, V is the DC voltage, and L_{e1}, L_{e2}, and L_{e3} are the external inductances. When the phase shift control signal for the full bridge cell of the primary port is the reference signal, δ_2 [rad] is the phase shift of the control signals between the primary and secondary ports, and δ_3 [rad] is the phase shift of the control signals between the primary and tertiary ports. When the three-winding transformer, the external inductors, and SiC-MOSFETs are ideal components, the basic equations of transmission power P_1, P_2, and P_3 are given by equations (1), (2), and (3), where $A = L_{e1}L_{e2} + L_{e2}L_{e3} + L_{e3}L_{e1}$ [15].

$$P_2 = \frac{\delta_2 (\pi - |\delta_2|) V_1 V_2 L_{e3} + (\delta_2 - \delta_3)(\pi - |\delta_2 - \delta_3|) V_2 V_3 L_{e1}}{2\pi^2 f_{sw} A} \quad \cdots\cdots (1)$$

$$P_3 = \frac{\delta_3 (\pi - |\delta_3|) V_1 V_3 L_{e2} + (\delta_3 - \delta_2)(\pi - |\delta_3 - \delta_2|) V_2 V_3 L_{e1}}{2\pi^2 f_{sw} A} \quad \cdots\cdots (2)$$

$$P_1 + P_2 + P_3 = 0 \quad \cdots\cdots (3)$$

As shown in equations (1) and (2), δ_2 and δ_3 are the control variables for the transmission power of each port. When the

transmission power of two of the three ports is determined, the other can be determined automatically.

3. Decoupling Power Flow Control System

This section describes the closed-loop power flow control system with decoupling power control of the TAB converter, hereinafter called the decoupling power flow control system. In this system, two port currents of the converter I_{2_conv} and I_{3_conv} are the control objectives. Here, $I_{2\_conv} = P_2/V_2$ and $I_{3\_conv} = P_3/V_3$.

The mathematical model of the control objective is generally essential to construct the feedback control system. Constructing the decoupling power flow control system includes three difficulties. First, equations (1) and (2) are not linear for δ_2 and δ_3. Second, equations (1) and (2) have six variations due to the magnitude relationship of δ_2 and δ_3. Third, P_2 and P_3 are the two-variable functions of δ_2 and δ_3, as shown in equations (1) and (2), i.e., the variation in transmission power of one port interferes with other ports. Therefore, to construct the system, we need linear models established regardless of the magnitude relationship of δ_2 and δ_3. Moreover, decoupling control is needed to eliminate the interference between the secondary port's control and the tertiary port's control.

Numerous studies about averaging methods of switching converters have been reported [16]-[20]. However, the conventional state-space averaging method is difficult to adapt for the TAB converter because the integral value of the external inductor current over one cycle is zero. Therefore, in this paper, the dynamics of all passive components in the TAB converter are neglected, and the transfer function of the control-to-output is obtained from basic equations, which are established with low operating speed.

First, the sinusoidal approximation shown in equation (4) is applied to equations (1) and (2) to enable these equations to be made regardless of the magnitude relationship of δ_2 and δ_3.

$$\delta(\pi - |\delta|) \approx X \sin\delta \cdots\cdots (4)$$

Here, the constant X can be derived by calculating the Fourier coefficient, as shown in (5).

$$X = \frac{1}{\pi}\int_{-\pi}^{\pi} \delta\,(\pi - |\delta|)\sin\delta\, d\delta = \frac{8}{\pi} \cdots\cdots (5)$$

Then, the basic equations of converter currents become equations (6) and (7).

$$I_{2\_conv} = \frac{P_2}{V_2} = \frac{4(V_1 L_{e3}\sin\delta_2 + V_3 L_{e1}\sin(\delta_2 - \delta_3))}{\pi^3 f_{sw} A} \cdots\cdots (6)$$

$$I_{3\_conv} = \frac{P_3}{V_3} = \frac{4(V_1 L_{e2}\sin\delta_3 + V_2 L_{e1}\sin(\delta_3 - \delta_2))}{\pi^3 f_{sw} A} \cdots\cdots (7)$$

Four solutions of δ_2 and δ_3 satisfying the command value can be obtained from equations (1) and (2) at maximum. However, the solution with the lowest conduction loss is close to the origin on the δ_2-δ_3 plane [14]. Therefore, the linear approximation around the origin on the δ_2-δ_3 plane is applied to equations (6) and (7) to construct a linear system. As a result, the linear model of the TAB converter, which includes converter currents I_{2_conv} and I_{3_conv}, becomes equation (8).

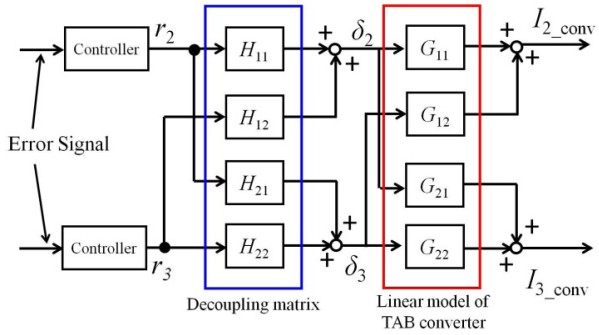

Fig. 5. Block diagram for a decoupling process

$$\begin{bmatrix} I_{2\_conv} \\ I_{3\_conv} \end{bmatrix} = G \begin{bmatrix} \delta_2 \\ \delta_3 \end{bmatrix} = \begin{bmatrix} \dfrac{4(V_3 L_{e1} + V_1 L_{e3})}{\pi^3 f_{sw} A} & \dfrac{-4 V_3 L_{e1}}{\pi^3 f_{sw} A} \\ \dfrac{-4 V_2 L_{e1}}{\pi^3 f_{sw} A} & \dfrac{4(V_2 L_{e1} + V_1 L_{e2})}{\pi^3 f_{sw} A} \end{bmatrix} \begin{bmatrix} \delta_2 \\ \delta_3 \end{bmatrix} \cdots\cdots (8)$$

As shown in equation (8), I_{2_conv} and I_{3_conv} interfere. By considering the inverse matrix of G, the interference can be eliminated. δ_2 and δ_3 are defined as equation (9) with medium variations r_2, r_3, and the matrix H, which is the inverse matrix of G.

$$\begin{bmatrix} \delta_2 \\ \delta_3 \end{bmatrix} = H \begin{bmatrix} r_2 \\ r_3 \end{bmatrix} = G^{-1} \begin{bmatrix} r_2 \\ r_3 \end{bmatrix} \cdots\cdots (9)$$

By substituting equation (9) into (8), both I_{2_conv} and I_{3_conv} become the one-variable functions of r_2 and r_3. That is, the transmission power of each port can be controlled independently because the interference between I_{2_conv} and I_{3_conv} is eliminated by matrix H. The decoupling matrix H is given by equation (10), where $B = V_3 L_{e1} L_{e2} + V_1 L_{e2} L_{e3} + V_2 L_{e3} L_{e1}$.

$$H = \frac{1}{B}\begin{bmatrix} \dfrac{\pi^3 f_{SW} A(V_1 L_{e2} + V_2 L_{e1})}{4 V_1} & \dfrac{\pi^3 f_{SW} A V_3 L_{e1}}{4 V_1} \\ \dfrac{\pi^3 f_{SW} A V_2 L_{e1}}{4 V_1} & \dfrac{\pi^3 f_{SW} A(V_1 L_{e3} + V_3 L_{e1})}{4 V_1} \end{bmatrix} \cdots\cdots (10)$$

The block diagram of the decoupling process is shown in Fig. 5, and the equation becomes (11).

$$\begin{bmatrix} I_{2\_conv} \\ I_{3\_conv} \end{bmatrix} = \begin{bmatrix} G_{11} & G_{12} \\ G_{21} & G_{22} \end{bmatrix} \begin{bmatrix} H_{11} & H_{12} \\ H_{21} & H_{22} \end{bmatrix} \begin{bmatrix} r_2 \\ r_3 \end{bmatrix} \cdots\cdots (11)$$

4. Implementation of the System

The decoupling power flow control system proposed in Section 3 was implemented in a 32-bit, 60 MHz microcomputer, RX64M (Runesas). The micro-computer calculated the value of phase shifts δ_2 and δ_3 with a switching frequency f_{sw} of 20 kHz. The DC output currents and voltages were sampled using an internal 12-bit A/D converter with a sampling frequency of 83 kHz.

Figure 6 shows the implemented TAB converter, Table 1 lists the specifications, and Fig. 7 shows the implemented

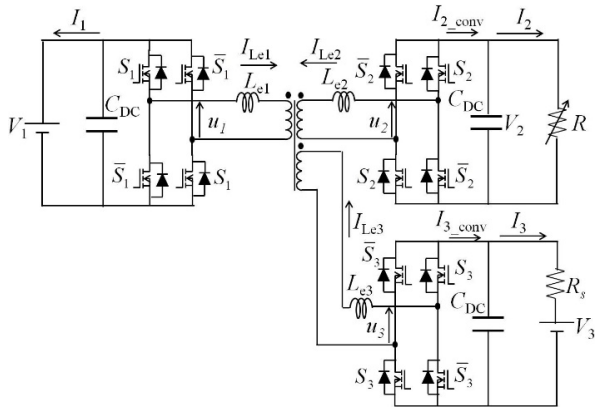

Fig. 6. Implemented TAB converter

Table 1. Specifications of prototype TAB converter

DC voltage [V]	V_1 ,V_3	400
Switching frequency [kHz]	f_{sw}	20
Rated power [kW]	P_R	10
Turn ratio of transformer		1:1:1
DC capacitor [mF]	C_{DC}	9.4
External inductances [μH]	L_e	41.2, 39.7, 40.5
Proportional gain of voltage control loop	K_{p_V2}	0.547
Integral time constant of voltage control loop [ms]	T_{i_V2}	200
Integral time constant of current control loop [ms]	T_{i_I3}	25

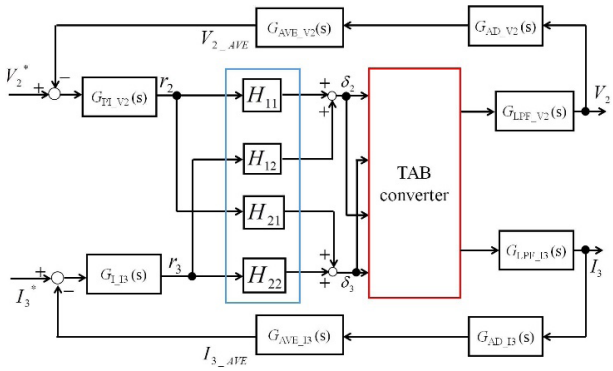

Fig. 7. Block diagram of implemented decoupling power flow control system

control loops of the decoupling power flow control system. Primary and tertiary ports' voltages V_1 and V_3 were regulated to 400 [V] using the external voltage source in Fig. 6, and the converter controlled the output current of the tertiary port I_3. However, the secondary port was connected to load R, and the converter controlled its output voltage V_2. $G_{\mathrm{LPF\_V2}}$(s) and $G_{\mathrm{LPF\_I3}}$(s) are the transfer functions of the low pass filters. These filters output the V_2 and I_3, as shown in equations (12) and (13).

$$V_2 = G_{LPF\_v2}(s)\, I_{2\_conv} = \frac{R}{1 + sRC_{DC}} I_{2\_conv} \cdots\cdots (12)$$

$$I_3 = G_{LPF\_I3}(s)\, I_{3\_conv} = \frac{1}{1 + sR_sC_{DC}} I_{3\_conv} \cdots\cdots (13)$$

$G_{\mathrm{AD\_V2}}$ (s) and $G_{\mathrm{AD\_I3}}$ (s) represent the A/D converter's delays, which are the sample and hold time in the A/D converter and conversion time. The sum of the A/D converter's delays is 2.0 μs. $G_{\mathrm{AVE\_V2}}$(s) and $G_{\mathrm{AVE\_I3}}$ (s) are the transfer functions of the moving average with 16 points. These moving average blocks output V_{2_AVE} and I_{3_AVE}. In this implemented system, only the output voltage of secondary port V_2 is a variable in equation (9) because the other ports' voltages were fixed to 400 [V] using external voltage sources. Therefore, the decoupling matrix H was calculated using each switching period with the specifications shown in Table 1 and V_{2_AVE} to obtain matrix H accurately. $G_{\mathrm{PI\_V2}}$ (s) represents the PI controller for regulating the output voltage V_2, and $G_{\mathrm{I\_I3}}$ (s) is the integral controller to manage the output current of tertiary port I_3. They needed to be discretized to implement them into a micro-computer. In this system, the controllers are written as shown in equations (14) and (15) using the backward Euler method.

$$r_2[n] = K_{p\_V2}\left(V_2^* - V_{2_{AVE}}[n]\right) + \sum_{k=0}^{n} \frac{\left(V_2^* - V_{2_{AVE}}[k]\right)}{f_{SW} \times T_{i\_V2}} \cdots\cdots (14)$$

$$r_3[n] = \sum_{k=0}^{n} \frac{\left(I_3^* - I_{3\_AVE}[k]\right)}{f_{SW} \times T_{i\_I3}} \cdots\cdots (15)$$

5. Experimental Results

This section reports the experimental results for the prototype TAB converter, in which the decoupling power flow control system was implemented. Figure 8(a) shows the prototype, and Fig. 8(b) shows the external inductors and three-winding transformer. The circuit configuration and parameters are shown in Fig. 6 and Table 1, respectively. The primary and tertiary ports' voltages were fixed to 400 V using external voltage sources, and the output current of the tertiary port I_3 was controlled. However, the secondary port was connected to load R, and its output voltage V_2 was controlled.

Figure 9 shows the experimental results with the decoupling power flow control system. In the first state, the load R = 180 Ω was connected to the secondary port, and the command value of the secondary port $V_2{}^*$ = 400 V. However, the command value of the tertiary port $I_3{}^*$ = 8.0 A. In this state, the voltage of the secondary port was kept at 400 V, and the current of the tertiary port was 7.9 A. The transmission power through the secondary and tertiary ports was 0.80 and 3.16 kW, respectively. In the second state, the load R was changed to 45 Ω from 180 Ω. The command values of both ports were the same as those in the first state. The current through the secondary port became 8.9 A. The voltage was decreased to 391 V at once, and it recovered to 400 V within 100 ms. At the same time, the current through the tertiary port was regulated to be constant. In this state, the transmission power through the secondary and tertiary ports was 3.56 and 3.16 kW. In the final state, the command value of the tertiary port $I_3{}^*$ was changed to 16.0 A from 8.0 A, and the load connected to the secondary port was the same as that in the second state. In this state, the transmission power through the secondary and tertiary ports was 3.56 and 6.24 kW. I_3 was changed to the command value with no overshoot, and the time constant T_d was 25.1 ms. Moreover, interference between the secondary port control and tertiary port control

(a)

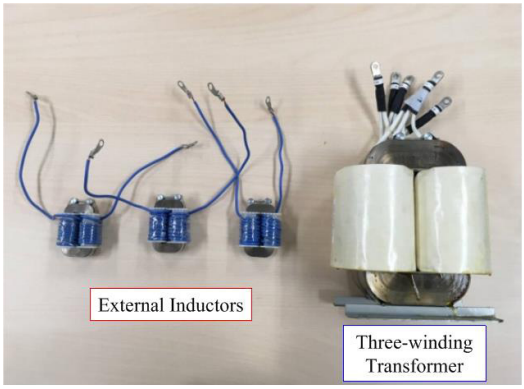

(b)

Fig. 8. (a) Prototype TAB converter (b) Three-winding transformer and external inductors

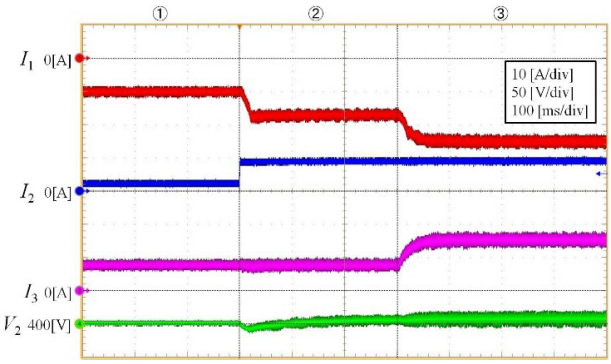

Fig. 9. Experimental results with decoupling matrix

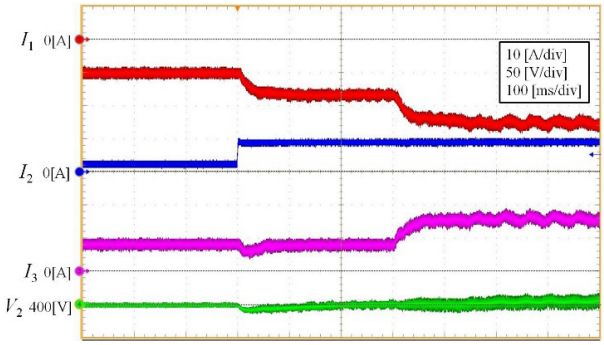

Fig. 10. Experimental results without decoupling matrix

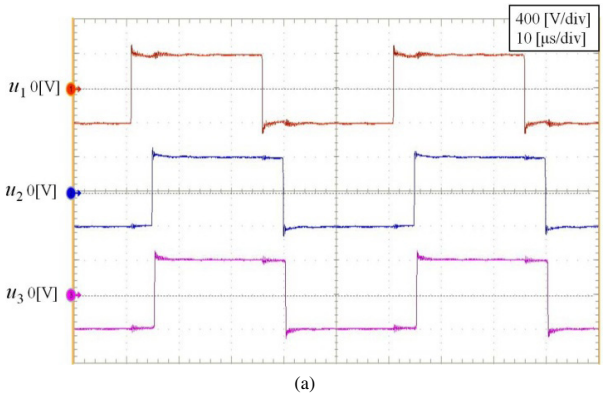

(a)

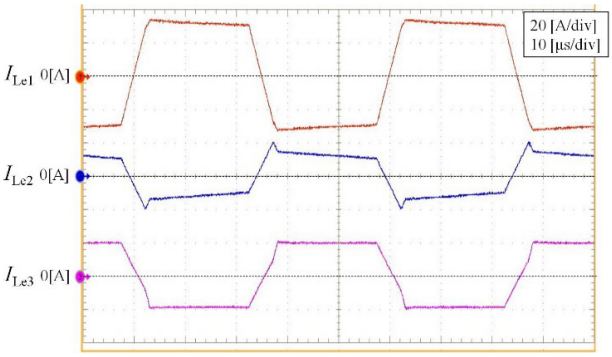

(b)

Fig. 11. (a) Waveforms of inverter voltages (b) Waveforms of inverter currents

was not observed. Some bit error was evident between the command value and measured value of the DC current and voltages. This was due to an error in the calibration of the measurement system for the prototype TAB converter.

As shown in Fig. 10, the interference between the secondary port control and tertiary port control was observed when the decoupling matrix H was not installed. All conditions were the same except for the decoupling matrix H. When the decoupling matrix was not active, the secondary port control varied only δ_2, and the tertiary port control varied only δ_3. At the beginning of the second state, I_3 was decreased to 5.5 A under the same command value $I_3{}^* = 8.0$ A. Namely, I_3 was decreased by 30% due to the interference.

Figure 11(a) and (b) show the steady states of inverter voltage u_1, u_2, and u_3 and inverter currents I_{Le1}, I_{Le2}, and I_{Le3} in the final state. The phase shifts δ_2 and δ_3 were 0.59 and 0.71 [rad], respectively. These phase shifts regulated to the solutions were close to the origin on the δ_2-δ_3 plane. That is, the system operated with the lowest conduction losses. As shown in Fig. 11(b), the biased magnetization of the external inductors and three-winding transformer were not observed.

These experimental results show that the implemented TAB converter can control both the voltage and current. In addition, the decoupling power flow control system was effective in eliminating the interference. Namely, the microgrid shown in Fig. 3 can be constructed by utilizing TAB converters.

6. Conclusion

A decoupling power flow control system that can manage the power flow between three ports was designed and implemented in a prototype triple active bridge (TAB) converter rated at 400 V, 10 kW, and 20 kHz. The validity of the system was demonstrated by measuring the step response of the TAB

converter. The experimental results showed that the system provided the designed dynamic characteristics from the viewpoint of output current control and constant voltage control. Decoupling power flow control between each port was also achieved.

Both voltage and current controls are essential functions of a TAB converter to construct autonomous DC microgrid systems with multi-TAB converters. Therefore, our test through the stand-alone operation of the TAB converter revealed that a prototype of the DC microgrid can be constructed using TAB converters with the decoupling power flow control system that we developed.

Acknowledgment

This work was supported by JSPS KAKENHI Grant Number JP16KT0104.

References

(1) H. Saitoh, S. Miyamori, T. Shimada, and J. Toyoda: "A study on autonomous decentralized control mechanism of power flow in open electric energy network", *IEEJ Trans. PE*, Vol.117, No.1, pp.10–18 (1997)

(2) A. Huang, M. Crow, G. Heydt, J. Zheng, and S. Dale: "The future renewable electric energy delivery and management (FREEDM) system: the energy internet", Proc. IEEE, Vol.99, pp.134–148 (2011)

(3) R. Abe, H. Taoka, and D. McQuilkin: "Digital grid: communicative electrical grids of the future", *IEEE Trans. Smart Grid*, Vol.2, No.2, pp.399–410 (2011)

(4) Y. Xu, J. Zhang, W. Wang, A. Juneja, and S. Bhattacharya: "Energy router: architectures and functionalities toward energy internet", Proc. IEEE Smart Grid Communications Conf., pp.31–36 (2011)

(5) Z. Wang and H. Li: "An Integrated Three-Port Bidirectional DC-DC Converter for PV Application on a DC Distribution System", *IEEE Trans. Power Electronics*, Vol.28, No.10, pp.4612–4624 (2013)

(6) S. Bahrami, V.W.S. Wong, and J. Jatskevich: "Optimal Power Flow for AC-DC Networks", IEEE Int. Conf. on Smart Grid Communications (2014)

(7) P. Khamphakdi, K. Sekiguchi, M. Hagiwara, and H. Akagi: "A Transformerless Back-To-Back (BTB) System Using Modular Multilevel Cascade Converters For Power Distribution Systems", *IEEE Trans. on Power Electronics*, Vol.30, No.4, pp.1866–1875 (2015)

(8) M. Neubert, A. Gorodnichev, J. Gottschlich, and R.W. De Doncker: "Performance Analysis of a Triple-Active Bridge Converter for Interconnection of Future DC-Grids", IEEE Energy Conversion Congress and Exposition (2016)

(9) R. Chattopadhyay and S. Bhattacharya: "ZVS Analysis and Power Flow Control for Three Limb Transformer Enabled SiC Mosfet Based Three Port DAB Integrating PV and Energy Storage (ES)", IEEE Energy Conversion Congress and Exposition (2016)

(10) S. Inoue and H. Akagi: "A Bi-directional Isolated DC/DC Converter as a Core Circuit for 3.3-kV/6.6-kV Power Conversion Systems in the Next Generation", IEEE Power Electronics Specialists Conference (PESC), Vol.126, No.3, pp.211–217 (2006)

(11) Y. Kado, D. Shichijo, K. Wada, and K. Iwatsuki: "Multiport power router and its impact on future smart grids", Radio Science, Vol.51, No.7, pp.1234–1246 (2016) DOI: 10.1002/2016RS006041.

(12) J.-C. Choi, H.-Y. Jeong, J.-Y. Choi, D.-J. Won, S.-J. Ahn, and S.-Il Moon: "Voltage Control Scheme with Distributed Generation and Grid Connected Converter in a DC Microgrid", Energies, Vol.7, No.10, pp.6477–6491 (2014) DOI: 10.3390/en7106477.

(13) Y. Kado, R. Kasashima, N. Iwama, and K. Wada: "Implementation and Performance of Three-way Isolated DC/DC Converter using SiC-MOSFETs for Power Flow Control", Proc. IEEE Int. Power Electronics for Distributed Generation Systems Conf. (2016) DOI: 10.1109/PEDG.2016.7527102.

(14) Y. Kado, D. Shichijo, I. Deguchi, N. Iwama, R. Kasashima, and K. Wada: "Power flow control of three-way isolated DC/DC converter for Y-configuration power router", Proc. IEEE Int. Future Energy Electronics Conf., Paper No.290294 (2015) DOI: 10.1109/IFEEC.2015.7361500.

(15) C. Zhao, S.D. Round, and J.W. Kolar: "An isolated three-port bidirectional DC-DC converter with decoupled power flow management", *IEEE Trans. Power Electron.*, Vol.23, No.5, pp.2443–2453 (2008)

(16) B. Zhao, Q. Song, W. Liu, and Y. Sun: "Overview of Dual-Active-Bridge Isolated Bidirectional DC–DC Converter for High-Frequency-Link Power-Conversion System", *IEEE Trans. Power Electronics*, Vol.29, No.8, pp.4091–4106 (2014)

(17) C. Zhao, S.D. Round, and J.W. Kolar: "Full-order averaging modelling of zero-voltage-switching phase-shift bidirectional DC-DC converters", *IET Power Electronics*, Vol.3, No.3, pp.400–410 (2010)

(18) F. Krismer and J.W. Kolar: "Accurate Small-Signal Model for the Digital Control of an Automotive Bidirectional Dual Active Bridge", *IEEE Trans. on Power Electronics*, Vol.24, No.12, pp.2756–2768 (2009) DOI: 10.1109/TPEL.2009.2027904.

(19) S.R. Sanders, J.M. Noworolski, and G.C. Verghese: "Generalized averaging method for power conversion circuits", *IEEE Trans. on Power Electronics*, Vol.6, No.2, pp.251–259 (1991) DOI: 10.1109/63.76811.

(20) H. Qin and J.W. Kimball: "Generalized Average Modeling of Dual Active Bridge DC-DC Converter", *IEEE Trans. on Power Electronics*, Vol.27, No.4, pp.2078–2084 (2012)

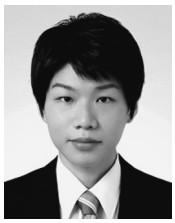

Koya Nishimoto (Non-member) received a B.S. Degree in the Department of Electronics from the Kyoto Institute of Technology, Kyoto, Japan, in 2016. He is currently working toward an M.S. degree in the Department of Electronics, Kyoto Institute of Technology. His current research interests include triple active bridge converters.

Yuichi Kado (Non-member) received M.S. and Ph.D. degrees in electronics from Tohoku University, Miyagi, Japan, in 1983 and 1998. In 1983, he joined the Electrical Communication Laboratories of the Nippon Telegraph and Telephone Public Corporation (now NTT), Kanagawa, Japan, where he was engaged in research on SOI structure formation by hetero-epitaxial growth. From 1989 to 1998, he worked on the development of fully depleted CMOS/SIMOX LSIs and ultra-low-power CMOS circuits. Starting in 1999, he was engaged in R&D on compact network appliances using ultralow-power CMOS circuit technologies for ubiquitous communications. He led research and development projects on ultra-low-power network appliances, sub-terahertz-wave wireless communication, and intra-body communication as a director of the Smart Devices Laboratory at NTT Microsystem Integration Laboratories (2003–2010). In July 2010, he joined the Department of Electronics, Kyoto Institute of Technology, Kyoto, Japan. His current research interests include multi-port power routers to build energy interchanging systems. He has been the recipient of awards including the 2009 Nikkei BP Technology Award, the 2009 Radio wave Achievement Award presented by the ARIB, and the 2009 Telecom System Technology Award presented by the Telecommunications Advancement Foundation. He is a board member of NPERC-J (http://www.nperc-j.or.jp) and a member of IEEE.

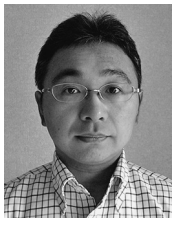

Keiji Wada (Senior Member) received a Ph.D. degree in electrical engineering from Okayama University, Okayama, Japan, in 2000. From 2000 to 2006, he was a Research Associate with Tokyo Metropolitan University, Tokyo, Japan, and the Tokyo Institute of Technology, Tokyo. Since 2006, he has been an Associate Professor in Tokyo Metropolitan University. His current research interests include medium-voltage inverters, electromagnetic interference filters, and active power filters.